Desalination and Water Treatment
www.deswater.com

doi: 10.5004/dwt.2019.23510

140 (2019) 347–355
February

Adsorption of methylene blue by graphene immobilized cross-linked chitosan beads

Baixiang Ren[a,*], Xiaoyue Duan[a,b,*], Yinan Wang[a]

[a]*Key Laboratory of Environmental Materials and Pollution Control, Education Department of Jilin Province, Siping 136000, China, Tel. +86 434 3290623; Fax: +86 434 3292233; emails: renbaixiang0105@163.com (B. Ren), duanxiaoyue0511@163.com (X. Duan), 736683643@qq.com (Y. Wang)*
[b]*Key Laboratory of Preparation and Application of Environmental Friendly Materials, Ministry of Education, Jilin Normal University, Siping 136000, China*

Received 7 May 2018; Accepted 21 November 2018

ABSTRACT

In this study, an effective bio-adsorbent of graphene immobilized cross-linked chitosan (GCCT) beads were successfully prepared by entrapping graphene in cross-linked chitosan. The adsorbents were characterized by scanning electron microscope, Fourier infrared spectroscopy and N_2 adsorption–desorption isotherms. Batch adsorption experiments were performed to remove cationic dye, methylene blue (MB), in aqueous solution using GCCT beads. The effect of initial MB concentration (10–90 mg/L) and temperature (25°C–65°C) on the adsorption removal of MB was evaluated. The adsorption kinetics, isotherm, mechanism and thermodynamics were also discussed. The results showed that the graphene immobilization over the chitosan significantly improved the specific surface area of chitosan beads. Thus, the GCCT beads presented a remarkable enhancement of adsorption capacity for the removal of MB from the aqueous solution. The kinetics of adsorption of MB followed the pseudo-second kinetics equation, and the equilibrium data were better analyzed by Freundlich isotherm model. At the temperature of 65°C, the Freundlich maximum multilayer adsorption capacity of GCCT beads for 90 mg/L MB was 7.64 mg/g. Adsorption diffusion model stated that the present adsorption was not only controlled by the intraparticle diffusion. The thermodynamic parameters showed that the present adsorption was a spontaneous and endothermic process. Overall, the GCCT beads have proved a promising adsorbent for removal of dyes from aqueous solution.

Keywords: Methylene blue; Graphene; Chitosan; Adsorption

1. Introduction

Dyes are excessively used in diverse consumer products, such as textile, painting, paper, food, leather, pharmaceutical, etc. [1]. Due to the wide usage of dyes, approximately, 200,000 tons of wastewater contaminated by dyes is discharged into the effluents annually, causing serious environmental and health problems [2]. Among various dyes, the cationic dyes are considered to be of the highest toxicity [3]. Methylene blue (MB), as one of the basic cationic dyes, has been widely used in printing and dyeing industries [4]. However, the exposure of MB for long term may cause irritation, vomiting, diarrhea, nausea, severe headache, mental confusion and profuse sweating [1,5]. Therefore, it becomes mandatory to treat the MB contained effluents before discharging them into aqueous environment to avoid or reduce the water pollution. In previous studies, a large number of technologies have been used to treat dye wastewater. Adsorption technology is most commonly used to remove dyes from wastewater because of its low cost, high efficiency and easy operating. Various adsorbents have been adopted for removing dye from wastewater, including carbon materials [1], clay minerals [6], biopolymers [7], and so on. However, it is

* Corresponding authors.

1944-3994/1944-3986 © 2019 Desalination Publications. All rights reserved.

difficult to recycle these adsorbents from treated wastewater due to their small size and excellent dispersing property in aqueous solution. Thus, the magnetic and granular adsorbents have been developed and applied in recent studies.

Chitosan (CT), a cheap, non-toxic, biocompatible and effective bio-adsorbent containing abundant amino ($–NH_2$) and hydroxyl (–OH) groups, has been widely used for removal of dyes, but the application of CT is limited by its dissolution in acid solutions [7]. Fortunately, the CT hydrogel beads can be formed by cross-linking in NaOH solution, which renders the polymer insoluble in acidic media, thereby increasing its mechanical and chemical stability and making it much easier to recycle absorbent [8,9]. In order to further improve the mechanical property and adsorption capacity of CT beads, some composites have been added into the CT beads, including MnO_2 [10], montmorillonite [9], titania [11], activated oil palm ash zeolite [7], nano-ZnO [12]. In these studies, the composites appeared as effective materials for enhancing adsorption of dyes and heavy metal ions.

Graphene and graphene oxide are composed of two-dimensional sp^2 hybridized carbon network with a honeycomb lattice [13], which have been widely used in many fields due to their unique structure, outstanding mechanical, optical and electronic properties [14]. In addition, they also have the advantages of large specific surface area and high hydrophobic surface [15]. Thus, they also have been explored as a kind of effective adsorbent for the adsorption of organic contaminants from aqueous solution. Apul et al. [16] reported that graphene exhibited comparable or better adsorption capacity than carbon nanotubes and activated carbon. Rostamian and Behnejad [17] considered that the graphene oxide could be used as a more efficient adsorbent for the adsorption of sulfamethoxazole. In addition, the combination between graphene oxide and CT has been recently studied for adsorption of MB [13,18], which exhibited more advantages than CT beads and graphene oxide, including easy-to-recycle, high surface area, and high adsorption capacity. However, the synthesis and application of composites of graphene and CT for the removing of MB in the aqueous solution is rare in literature.

Thus, in this study, graphene was prepared by electrochemical exfoliation, and then the graphene immobilized cross-linked chitosan (GCCT) beads were synthesized and used for removing MB in aqueous solution. The surface morphology, functional group and structural analysis of adsorbents were conducted using scanning electron microscope (SEM), Fourier infrared spectroscopy (FTIR) and N_2 adsorption–desorption isotherms. The effect of initial MB concentrations and temperature was investigated. In addition, the adsorption kinetics, isotherms, mechanism and thermodynamics analysis were performed.

2. Materials and methods

2.1. Materials

Graphite sheets were purchased from Yichang Xincheng graphite products Co., Ltd. (China). CT, MB, acetic acid, glutaraldehyde and NaOH were purchased from Sinopharm Chemical Reagent Co., Ltd. (Shanghai, China). All of the chemicals were of analytical grade and were used without further purification.

2.2. Preparation of graphene

The graphene were fabricated by electrochemical exfoliation according to the reported method [19], which was performed in two-electrode system. A graphite sheet was employed as working electrode and a platinum plate was used as counter electrode. Applied cell potential was 10 V and the electrolyte was 0.4 wt% $(NH_4)_2SO_4$. Exfoliated floccules from anode surface were centrifuged and washed with ultrapure water repeatedly. Then the obtained graphene samples were dried in a vacuum oven at 60°C and stored after grinding.

2.3. Synthesis of GCCT beads

GCCT beads were synthesized according to the reported methods with some modification [7,8]. 6.0 g of CT was first dissolved in 100 mL of 10% v/v acetic acid solution under constant stirring. Then, 0.5 g of graphene powder and 0.5 mL of 25 wt% glutaraldehyde were added into CT solution and mechanically stirred for 12 h at room temperature. Thereafter, the CT solution containing graphene was dropped into the crosslinker solution of 0.5 mol/L NaOH solution using injector to form the GCCT beads. The obtained beads were matured for 24 h in the crosslinker solution. Finally, the synthesized GCCT beads were washed with ultrapure water up to neutral pH and dried at room temperature. The CT beads were also prepared without adding graphene for comparison.

2.4. Characterization of GCCT beads

The morphology of samples was characterized using SEM (JSM-6510, Japanese electronics) operated at 15 kV with a working distance of 13 mm. The functional groups on samples were analyzed by FTIR (Cary 630, Agilent) using KBr pellets method, the concentration of GCCT in which was 1% ± 0.02%. The FTIR spectra were collected in the region of 4,000–400 cm^{-1} with a resolution of 4 cm^{-1}. The N_2 adsorption/desorption experiment was carried out using a surface area and porosimetry system (3H-2000PS1, China) at 77 K. Before analysis, the samples were degassed at 150°C for 3 h. The Brunauer–Emmett–Teller (BET) and Barrett–Joyner–Halenda (BJH) methods were used to estimate the specific surface area and pore properties (pore volume and average pore diameter), respectively, on the basis of N_2 adsorption–desorption data.

2.5. Adsorption experiment

Adsorption experiments of MB were carried out by batch process and conducted in triplicate. The experimental studies were carried out at different initial MB concentrations (10–90 mg/L) and different temperatures (25°C–65°C). In each experiment, around 0.5 g of absorbent was added into 50 mL of MB solution in conical flake. The pH values of the MB solutions were unadjusted in all the experiments and the initial pH value of solutions were around 7.6. The adsorption mixture was agitated for the required time period in a water bath shaker. After the predetermined intervals, the samples were taken out from the conical flasks and the concentration of MB was determined by a UV-Vis spectrometer (TU-1810, China) at 662 nm. The adsorption capacity (q_e) of absorbent was calculated as:

$$q_e = \frac{(C_0 - C_e)V}{m} \quad (1)$$

where q_e is the equilibrium adsorption capacity (mg/g), C_0 and C_e are the concentration of MB (mg/L) at time zero and equilibrium (min), respectively, V is the solution volume (L) and m is the mass of absorbent (g).

3. Results and discussion

3.1. Morphology of GCCT beads

The CT and GCCT beads were spherical in shape with average diameters of around 0.6 cm. The microstructural studies of electrochemical exfoliated graphene, CT and GCCT beads were performed by SEM depicted in Fig. 1. The SEM image of graphene in Fig. 1(a) shows that the electrochemical exfoliated graphene has wrinkled sheet-like structure, which conformed to the basic shape of graphene, but its size was larger than those of graphene oxides synthesized using Hummers' method in literature [13,20]. The CT bead in Fig. 1(b) exhibits smooth surface, and nearly no porous structure is observed. Distinctive from the CT bead, the GCCT bead (Fig. 1(c)) displays a much rougher surface morphology. Comparing with graphene sheet, more wrinkles were observed on GCCT beads, and the edge of different graphene sheets appeared. These differences revealed that the CT had been aggregated on the surface of graphene sheets and the graphene sheets were broken. Thus, we deduced that the GCCT beads should have large surface area than CT beads, and then possess better adsorption capacity.

3.2. Functional group analysis

The FTIR spectra of graphene, CT and GCCT beads are shown in Fig. 2. For graphene, the peaks at 881; 1,079; 1,437; 1,637 and 3,437 cm^{-1} corresponded to the stretching vibration of O–C=O, C–O, C–OH, C=C and O–H bonds, respectively [21]. In CT spectrum, the strong band around 3,437 cm^{-1} was due to the stretching vibration of N–H and –OH groups and inter-molecular hydrogen bonds [22]. The typical bands of CT at 1,645 and 1,560 cm^{-1} were attributed to the amide I and amide II bonds, respectively [23]. The bond appeared at 1,435 cm^{-1} was ascribed to the bending of C–H [24]. The band of CT located at 1,082 cm^{-1} was related to the C–O stretching vibrations of C–OH and C–O–C groups in the glycosidic linkage [22]. The alcoholic group of C6–OH and the secondary alcohol group of C3–OH bands were also presented at 1,155 and 1,036 cm^{-1} in the CT spectrum [25]. Comparing with the IR spectrum of CT, the spectrum of GCCT showed broader peaks at around 1,630–1,560 cm^{-1} and stronger peaks at around 950–1,210 cm^{-1}, with a shift of 25 cm^{-1} for 1,435 cm^{-1} band. These differences demonstrated that the chitosan chains were successfully grafted onto the surface of graphene nanosheets via amide bonds. In addition, the increase of peak intensity may be associated to the overlapping of groups from graphene and CT.

3.3. Pore structure analysis

The pore structures of graphene, CT and GCCT beads were analyzed by N_2 adsorption–desorption isotherms. Fig. 3(a) shows the N_2 adsorption–desorption isotherms of three samples. According to IUPAC classification, all the adsorption–desorption curves presented typical characteristic of type-IV isotherms with a hysteresis loop at a high relative pressure, indicating the existence of mesoporous structure of all samples. The BET surface area, pore volume and average pore diameter results are summarized in Table 1. GCCT exhibited a surface of 33.85 m^2/g, which was lower than 46.00 m^2/g of graphene, but it was obviously

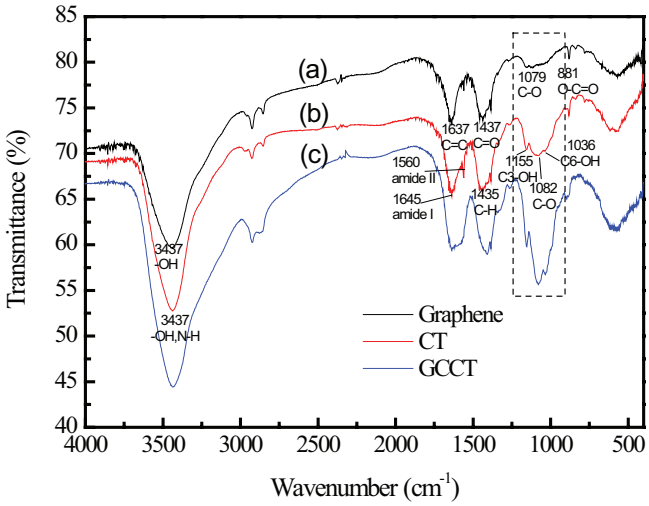

Fig. 2. FTIR spectra of graphene (a), CT bead (b) and GCCT bead (c).

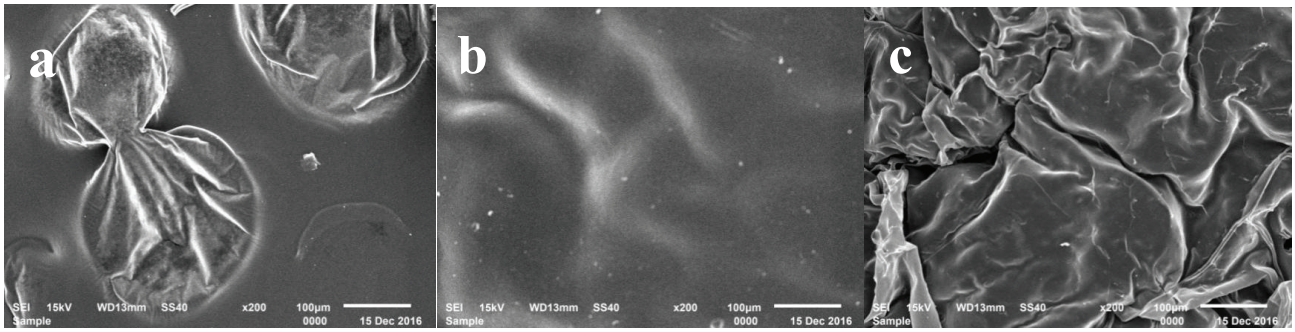

Fig. 1. SEM images of graphene (a), CT bead (b) and GCCT bead (c).

higher than that of CT (13.32 m^2/g). The pore size distribution of samples shown in Fig. 3(b) and Table 1 revealed that the pore sizes for graphene, CT and GCCT were all centralized at approximately 1.5–10 nm, and their average pore diameters were 9.4, 12.66 and 14.67 nm, respectively. Therefore, the graphene immobilization over the chitosan significantly improved the specific surface area, pore volume and pore diameter of CT beads, which contributed to enhancing the adsorption capacity of CT beads. According the above parameters, it should also be noted that the GCCT had a lower S_{BET} than graphene, but it presented larger pore volume and pore diameter. This may be due to that a small amount of large pores were formed between different graphene sheets during cross-linking process, which can remarkably enlarge the pore volume, but has little influence on specific surface area.

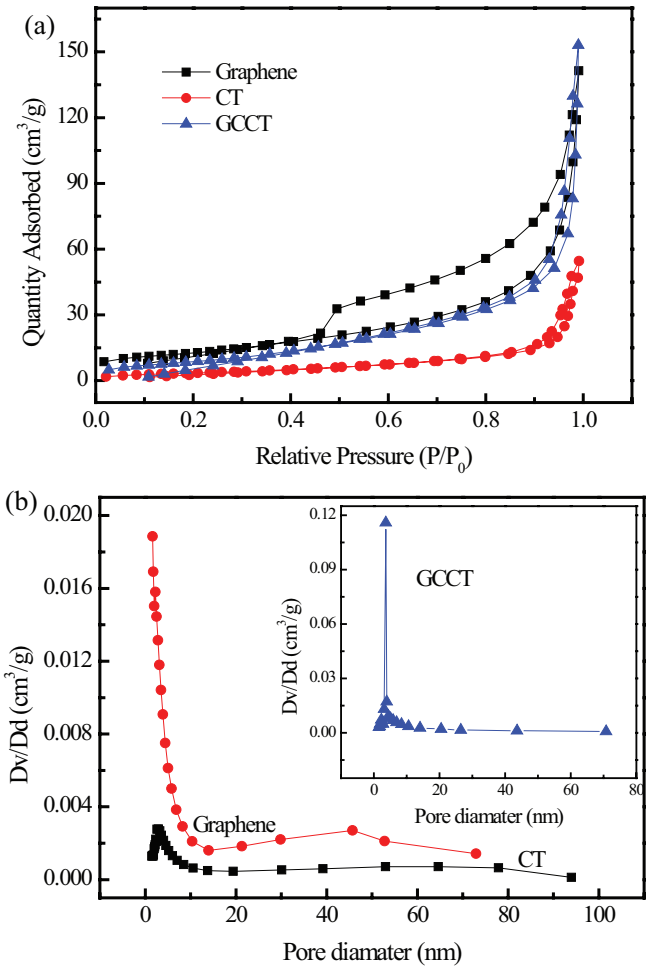

Fig. 3. N_2 adsorption–desorption isotherm (a) and pore size distribution (b) of graphene, CT bead and GCCT beads.

Table 1
BET surface area, pore volume and pore size for graphene, CT and GCCT beads

Sample	S_{BET} [a] (m^2/g)	V_{total} [b] (cm^3/g)	D_{ave} [c] (nm)
Graphene	46.00	0.2199	9.4
CT	13.32	0.0848	12.66
GCCT	33.85	0.2380	14.67

[a]Specific surface area (S_{BET}) was calculated by the BET method.
[b]V_{total} represented the total pore volume.
[c]Pore diameter D_{ave} is referred to the average pore size calculated by BJH method.

3.4. Adsorption of MB on graphene, CT and GCCT beads

The adsorption removal of MB on graphene, CT and GCCT beads was compared using batch-mode experiments at a constant initial MB concentration of 10 mg/L and the results are shown in Fig. 4. For all absorbents, the rapid removal was observed in the first 60 min. After that, the adsorption removal became slower because the large numbers of adsorption sites were occupied by MB. The adsorption equilibrium reached at about 240, 120 and 360 min for graphene, CT and GCCT beads, respectively. At equilibrium, MB removal was only 31.9% for CT beads, whereas 66.2% and 91.5% were obtained for graphene and GCCT beads, respectively. The adsorption capacities of graphene, CT and GCCT beads for MB were found to be 0.662, 0.319 and 0.915 mg/g, respectively. Therefore, the incorporation of graphene and CT not only was convenient for recycle of graphene but also improved the adsorption capacities of graphene and CT. However, this result seems to contradict the result of BET surface areas, in which the graphene had a higher surface area than GCCT beads. This contradiction may be explained by the larger pore volume and average pore size of GCCT than those of graphene and CT, which should contribute to the access of adsorption sites in the pores.

3.5. Effect of initial MB concentration and adsorption kinetics

Fig. 5(a) shows the effect of initial MB concentration on the adsorption removal of MB on GCCT beads. It is clear that, for all concentrations, the adsorption of MB on GCCT beads increased rapidly within the first 2 h, and then slowed down.

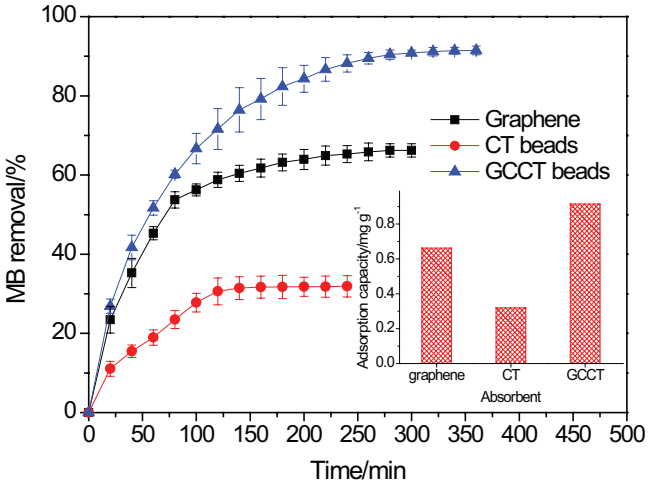

Fig. 4. Comparison of graphene, CT and GCCT beads for adsorption removal of MB. Inset shows the adsorption capacity of three absorbents. Adsorption condition: volume of solution = 100 mL; initial MB concentration = 10 mg/L, temperature = 25°C.

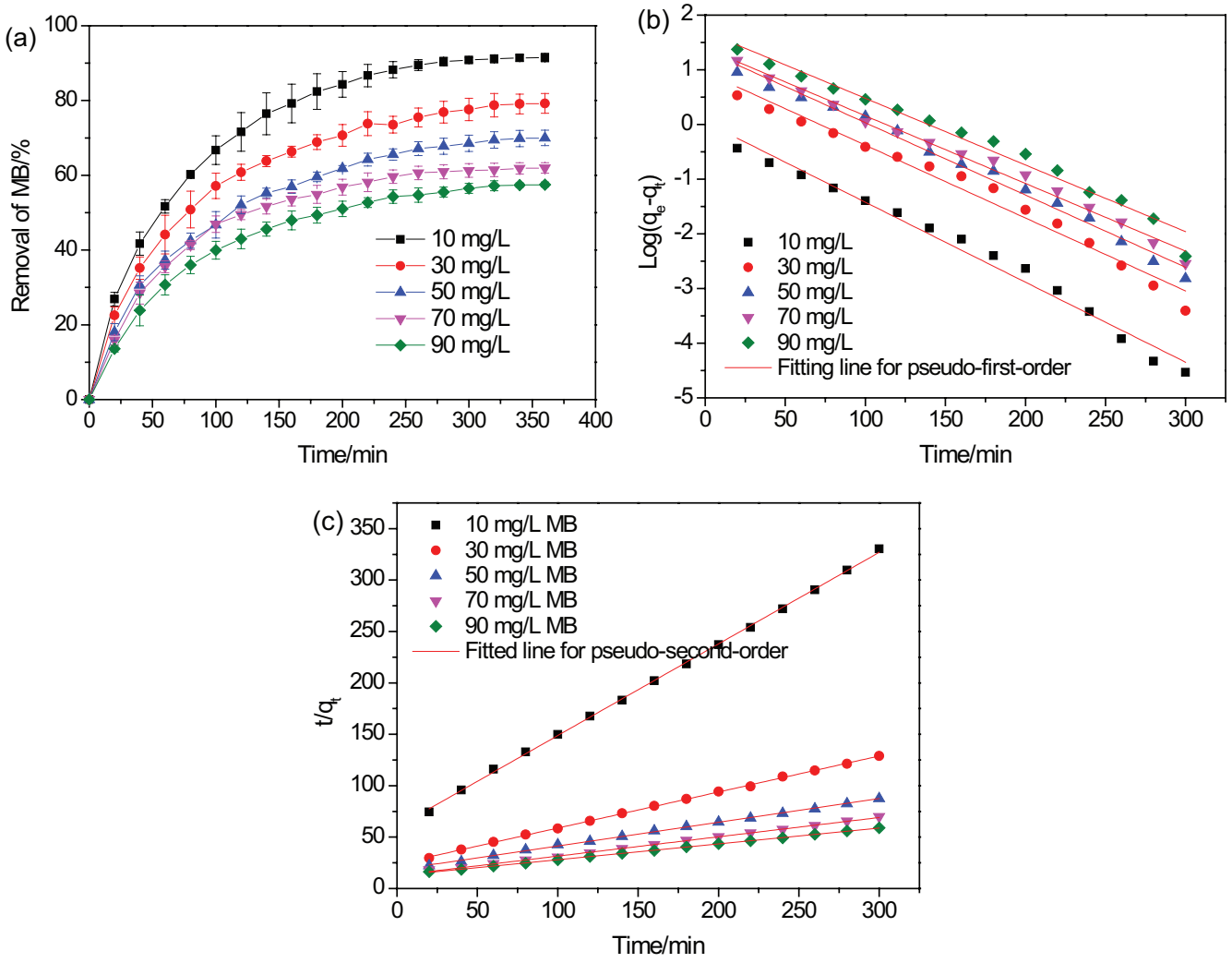

Fig. 5. MB removal efficiency (a), pseudo-first-order and pseudo-second-order models fitting curves ((b) and (c)) for MB adsorption at different initial concentrations. Adsorption condition: volume of solution = 100 mL; temperature = 25°C.

The removal efficiencies of MB were 91.5%, 79.2%, 70.0%, 62.0% and 57.5% at the adsorption equilibrium, and the corresponding adsorption capacities of MB were 0.91, 2.38, 3.50, 4.34 and 5.17 mg/g for 10, 20, 30, 40 and 50 mg/L of the initial concentration of MB, respectively. Therefore, the MB can be effectively removed by GCCT beads at different initial concentrations, and the removal efficiency of MB decreased and adsorption capacities of MB increased with increasing initial MB concentration from 10 to 90 mg/L. This was due to that more MB molecules were available and higher mass transfer driving force was attained for adsorption at a higher concentration of MB [26]. However, comparing the adsorption capacities with those in literature [7,15], it was found that the adsorption capacity of GCCT was lower, which may be owing to its big particle size and small specific surface area. It also may be related to the extremely high concentrations of MB in literature (up to 1,000 mg/L), and only 10–50 mg/L in our study. It is well known that smaller size of absorbent and high concentration of adsorbate will lead to higher sorption capacities [27]. In order to further understand the adsorption process, the adsorption data were determined using pseudo-first-order and pseudo-second-order adsorption kinetic equations, which are presented as [27,28]:

$$\log(q_e - q_t) = \log q_e - \frac{k_1}{2.303}t \tag{2}$$

$$\frac{t}{q_t} = \frac{1}{k_2 q_e^2} + \frac{t}{q_e} \tag{3}$$

where q_e and q_t are the amount of adsorbed MB (mg/g) at equilibrium and at time t (min), respectively, k_1 is the rate constant of pseudo-first-order (min^{-1}), and k_2 is the rate constant of pseudo-second-order (g/mg·min). Figs. 5(b) and (c) show the linear fitting curves between the equations and experimental data. The fitted parameters are presented in Table 2. It can be observed that the correlation coefficient (R^2) values for pseudo-second order kinetic model were closer to 1. In addition, the experimental values ($q_{e,exp}$) of the equilibrium sorption are also listed in Table 2 and they

Table 2
Kinetic parameters for the adsorption of MB on GCCT beads

Concentration (mg/L)	Pseudo-first-order model			Pseudo-second-order model			
	k_1 (min^{-1})	q_e (mg/g)	R^2	k_2 (g/mg·min)	q_e (mg/g)	R^2	$q_{e,exp}$ (mg/g)
10	0.0146	1.04	0.9829	0.0133	1.02	0.9994	0.91
20	0.0133	1.74	0.9770	0.0052	2.85	0.9995	2.38
30	0.0132	3.87	0.9886	0.0029	4.34	0.9986	3.50
40	0.0123	4.04	0.9903	0.0028	5.32	0.9986	4.34
50	0.0122	5.47	0.9776	0.0019	6.48	0.9996	5.17

were in good agreement with the calculated values ($q_{e,cal}$) from pseudo-second-order kinetic model. Consequently, the pseudo-second-order kinetic model is more proper for the adsorption process of MB on GCCT beads.

3.6. Adsorption mechanism

It is well known that the adsorption process includes three steps [29]: (i) diffusion of the adsorbate molecules from the bulk solution to the surface of absorbent, which is called film diffusion, (ii) diffusion of the adsorbate molecules from the surface of absorbent into the interior of pores of absorbent, which is called interior diffusion, (iii) adsorption of the adsorbate molecules on the interior surface of pores of absorbent, which is called adsorption. In order to understand the adsorption mechanism of MB on the GCCT beads, it is necessary to analyze the rate controlling step of adsorption process using Weber and Morris intraparticle diffusion model. The model is expressed as follows [30]:

$$q_t = k_p t^{\frac{1}{2}} + C \tag{4}$$

where q_t is the adsorption capacity (mg/g) at time t (min), k_p is the intraparticle diffusion rate constant (mg/g min$^{1/2}$) and C is the intercept. The fitting plots of q_t vs. $t^{1/2}$ are shown in Fig. 6. The first step was ascribed to the film diffusion. The second step corresponded to the intraparticle diffusion stage. From the slop and intercept of straight lines, values of k_p and C were estimated and are listed in Table 3. It can be observed that the fitting lines did not pass through the origin, suggesting the adsorption of MB on the GCCT beads was not only controlled by the intraparticle diffusion but also influenced by the steps of adsorption or film diffusion simultaneously. It also can be observed that the values of k_{pi} were larger than those of k_{pii}, demonstrating that film diffusion was a more rapid process than the intraparticle diffusion process.

3.7. Effect of temperature and adsorption isotherm

The effect of temperature on MB adsorption on GCCT beads is depicted in Fig. 7. For all the aqueous solution with the initial MB concentrations from 10 to 90 mg/L, the MB removal and adsorption capacity were increased with the temperature increasing from 25°C to 65°C. The maximum adsorption capacity of 7.64 mg/g was reached at the initial MB concentration of 90 mg/L and at the temperature of 65°C.

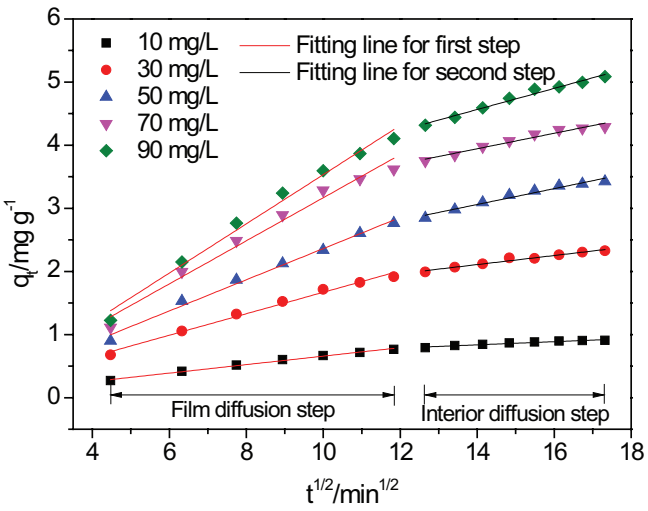

Fig. 6. Intraparticle diffusion fit for the adsorption of MB on GCCT beads.

To further understand the number of active sites undergone adsorption, equilibrium isotherms, including the Langmuir and Freundlich models, were chosen to fit the adsorption equilibrium data. The nonlinear expression of Langmuir and Freundlich can be expressed as [10] follows:

$$q_e = \frac{q_m K_L C_e}{1 + K_L C_e} \tag{5}$$

$$q_e = K_F C_e^{1/n} \tag{6}$$

where q_e is the amount of adsorbed MB at equilibrium (mg/g), C_e is the equilibrium concentration of MB solution (mg/L), q_m is the maximum monolayer adsorption capacity (mg/g), K_L is the Langmuir constant (L/mg), K_F is the Freundlich constant ((mg/g)(L/mg)$^{1/n}$), which is related to the adsorption capacity of the adsorbent and n is the Freundlich equation exponent. The adsorption capacities of GCCT beads vs. the equilibrium concentration of MB are plotted in Fig. 7(b). The parameters calculated from Langmuir and Freundlich models are listed in Table 4. The Freundlich model fitted the experimental data better than the Langmuir model with a higher determination coefficient for all temperatures, indicating the adsorption of MB on the surface of GCCT beads is multilayer adsorption,

Table 3
Intraparticle diffusion model fitting result for the adsorption of MB on GCCT beads

C_0 (mg/L)	Intraparticle diffusion model					
	Film diffusion step			Interior diffusion step		
	K_{pi} (mg/g min$^{1/2}$)	C_i	R^2	K_{pii} (mg/g min$^{1/2}$)	C_{ii}	R^2
10	0.0672	–0.0141	0.9930	0.0250	0.4868	0.9783
30	0.1701	–0.0311	0.9878	0.0718	1.1040	0.9589
50	0.2469	–0.1069	0.9894	0.1256	1.3024	0.9664
70	0.3412	–0.244	0.9764	0.1224	2.2302	0.9645
90	0.3899	–0.3650	0.9853	0.1673	2.2231	0.9577

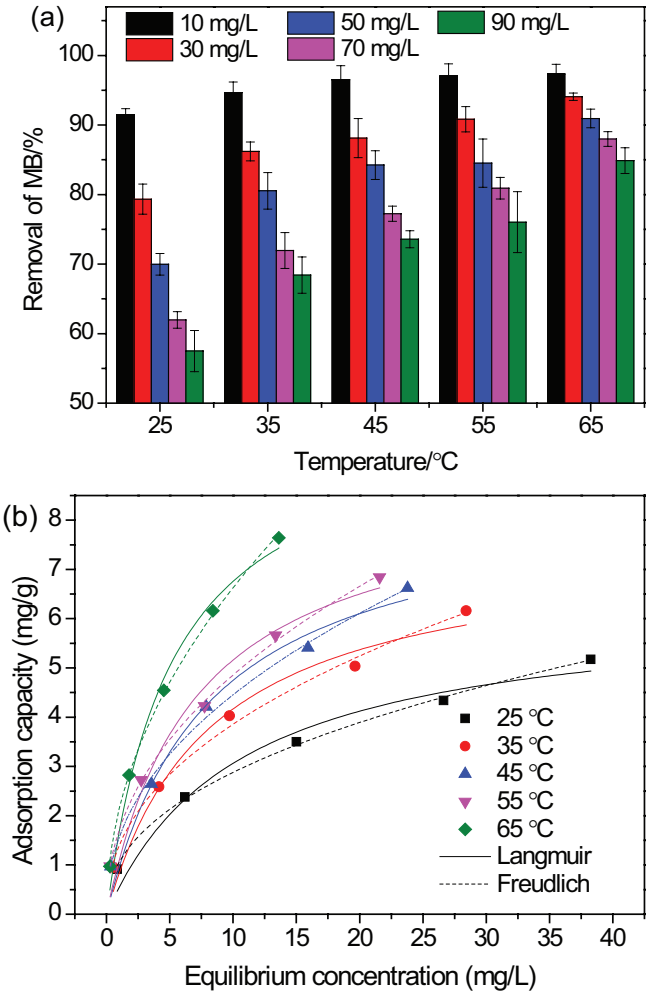

Fig. 7. Effect of temperature on the MB removal efficiency (a), Langmuir and Freundlich isotherm fitting curves for MB adsorption (b). Adsorption condition: volume of solution = 100 mL; initial MB concentration = 10–90 mg/L; temperature = 25°C–65°C.

and the heterogeneous and unequal adsorption pores are responsible for the adsorption process [31]. This result may be resulted from the inconsistent pore structure of CT and graphene in GCCT beads. Besides, this may be associated to multi-forces between GCCT beads and MB, such as electrostatic attraction force, van der Waals force, π–π interaction and hydrogen bond [32]. In addition, the value of n is an indicator of the degree of non-linearity between the solution concentration and adsorption [29]. It can be seen from Table 4 that, in this study all the values of n lied between 2 and 3. This indicates that the adsorption process of MB on GCCT beads was a physical process.

3.8. Thermodynamic studies

The thermodynamic parameters, including standard Gibbs free energy ($\Delta G°$), standard enthalpy ($\Delta H°$) and standard entropy ($\Delta S°$), were calculated by using the adsorption data at temperatures of 25°C, 35°C, 45°C, 55°C and 65°C. These parameters can be determined using the Gibbs isotherm [10] and Van't Hoff equation [33].

$$\Delta G° = \Delta H° - T\Delta S° \tag{7}$$

$$\Delta G° = -RT\ln K_c \tag{8}$$

where R is the perfect gas constant (8.314 J/mol K), T is the absolute temperature (K) and K_c is the equilibrium constant, which can be estimated using Eq. (9) [31].

$$K_c = \frac{C_{Ae}}{C_e} \tag{9}$$

where C_{Ae} is the amount of the adsorbed species adsorbed onto the adsorbent per litre of solution at equilibrium (mg/L).

The values of ΔH and ΔS were, respectively, determined from the intercept and slope of the plot of ΔG vs. T. In our study, the values of q_e and C_e for 50 mg/L of initial MB concentration were used to calculate the values of K_C.

The calculated adsorption thermodynamic parameters of MB on GCCT beads are shown in Table 5. The $\Delta G°$ values were found to be negative at all temperatures, indicating that spontaneous MB adsorption occurred on the GCCT beads [34]. More negative $\Delta G°$ values at higher temperatures demonstrated the adsorption was more favorable at higher temperature. $\Delta H°$ represents the change of heat after adsorption reaction. The positive $\Delta H°$ value for the adsorption of MB onto GCCT beads showed this adsorption process was endothermic. Therefore, the increase of temperature will be favorable for the adsorption process of MB from solution to GCCT beads. Besides, the $\Delta H°$ value (27.093 kJ/mol) was less than 40 kJ/mol, suggesting the present adsorption was physisorption process [35], which was in agreement with

Table 4
Isotherm parameters for the adsorption of MB on GCCT beads

Temperature (°C)	Langmuir			Freundlich		
	Q_m (mg/g)	K_L (L/mg)	R^2	K_F ($mg^{1-1/n}$ $L^{1/n}$/g)	n	R^2
25	6.2958	0.0948	0.9610	1.0574	2.2987	0.9981
35	7.5486	0.1232	0.9669	1.3911	2.2579	0.9931
45	8.5366	0.1253	0.9665	1.5591	2.1934	0.9949
55	8.7817	0.1542	0.9685	1.7051	2.1997	0.9989
65	10.2697	0.1924	0.9806	2.1252	2.0246	0.9985

Table 5
Thermodynamic parameters for the adsorption of MB on GCCT beads

Temperature (K)	ΔG (kJ/mol)	ΔH (kJ/mol)	ΔS (kJ/mol)	R^2
298	–2.466	27.093	0.099	0.952
308	–3.755			
318	–4.540			
328	–5.038			
338	–6.795			

the result of Freundlich model fitting. In addition, $\Delta S°$ represents the total entropy of the reaction. The positive $\Delta S°$ (0.099 kJ/mol) in present study illustrated the degree of freedom increased at MB–GCCT interface during the adsorption process [36].

4. Conclusion

The present study focused on the synthesis of newly graphene immobilized cross-linked chitosan bio-adsorbent and its application for the removal of MB from aqueous solution. The adsorbent was prepared by entrapping graphene in cross-linked CT and characterized using SEM, FTIR and N_2 adsorption–desorption isotherms analysis. The influence of initial MB concentration and temperature on adsorption capacity of GCCT beads was studied. With the increase of initial MB concentration and temperature, the adsorption capacity of GCCT beads obviously increased. The pseudo-first-order and pseudo-second-order models were adopted to analyze kinetic data. The data fitted better with the pseudo-second-order model. The adsorption process was also examined by adsorption isotherms of Langmuir and Freundlich isotherms and revealed that the Freundlich isotherm provide better fit with multilayer adsorption of MB on GCCT beads. The maximum adsorption capacity of 7.64 mg/g was reached at the initial MB concentration of 90 mg/L and temperature of 65°C. Weber and Morris intraparticle diffusion was used to analyze the adsorption of MB on the GCCT beads and presented that the adsorption process was not only controlled by the intraparticle diffusion. The thermodynamic parameters showed that the present adsorption was a spontaneous and endothermic process. Therefore, the synthesized GCCT beads can be effectively employed for the treatment of industrial dye wastewaters.

Acknowledgments

The authors would like to thank the financial support from the National Natural Science Foundation of China (Nos. 51778268 and 51808256), the Natural Science Fund Program of Jilin Province (No. 20180101192JC), the Science and technology Project of Jilin Education Bureau (No. JJKH20191026KJ), and the Open Funds of the State Key Laboratory of Rare Earth Resource Utilization (No. RERU2017010).

References

[1] Z. Ezzeddine, I. Batonneau-Gener, Y. Pouilloux, H. Hamad, Removal of methylene blue by mesoporous CMK-3: kinetics, isotherms and thermodynamics, J. Mol. Liq., 223 (2016) 763–770.
[2] J. Oliva, A.I. Martinez, A.I. Oliva, C.R. Garcia, A. Martinez-Luevanos, M. Garcia-Lobato, R. Ochoa-Valiente, A. Berlanga, Flexible graphene composites for removal of methylene blue dye-contaminant from water, Appl. Surf. Sci., 436 (2018) 739–746.
[3] V. Tharaneedhar, P. Senthil Kumar, A. Saravanan, C. Ravikumar, V. Jaikumar, Prediction and interpretation of adsorption parameters for the sequestration of methylene blue dye from aqueous solution using microwave assisted corncob activated carbon, Sustain. Mater. Technol., 11 (2017) 1–11.
[4] P. Senthil Kumar, R.V. Abhinaya, K. Gayathri Lashmi, V. Arthi, R. Pavithra, V. Sathyaselvaselvabala, S. Dinesh Kirupha, S. Sivanesan, Adsorption of methylene blue dye from aqueous solution by agricultural waste: equilibrium, thermodynamics, kinetics, mechanism and process design, Colloid J., 73 (2011) 651–661.
[5] P. Senthil Kumar, R. Sivaranjanee, U. Vinothini, M. Raghavi, K. Rajasekar, K. Ramakrishnan, Adsorption of dye onto raw and surface modified tamarind seeds: isotherms, process design, kinetics and mechanism, Desal. Wat. Treat., 52 (2014) 2620–2633.
[6] R. Zhu, Q. Zhou, J. Zhu, Y. Xi, H. He, Organo-clays as sorbents of hydrophobic organic contaminants: sorptive characteristics and approaches to enhancing sorption capacity, Clay. Clay Miner., 63 (2015) 199–221.
[7] W.A. Khanday, M. Asif, B.H. Hameed, Cross-linked beads of activated oil palm ash zeolite/chitosan composite as a bio-adsorbent for the removal of methylene blue and acid blue 29 dyes, Int. J. Biol. Macromol., 95 (2017) 895–902.
[8] E. Igberase, P. Osifo, Equilibrium, kinetic, thermodynamic and desorption studies of cadmium and lead by polyaniline grafted cross-linked chitosan beads from aqueous solution, J. Ind. Eng. Chem., 26 (2015) 340–347.
[9] F.A.R. Pereira, K.S. Sousa, G.R.S. Cavalcanti, D.B. França, L.N.F. Queiroga, I.M.G. Santos, M.G. Fonseca, M. Jaber, Green biosorbents based on chitosan-montmorillonite beads for anionic dye removal, J. Environ. Chem. Eng., 5 (2017) 3309–3318.
[10] V.P. Dinh, N.C. Le, L.A. Tuyen, N.Q. Hung, V.D. Nguyen, N.T. Nguyen, Insight into adsorption mechanism of lead(II) from aqueous solution by chitosan loaded MnO_2 nanoparticles, Mater. Chem. Phys., 207 (2018) 294–302.
[11] P.A. Nishad, A. Bhaskarapillai, S. Velmurugan, Enhancing the antimony sorption properties of nano titania-chitosan beads

using epichlorohydrin as the crosslinker, J. Hazard. Mater., 334 (2017) 160–167.
[12] S. Çınar, Ü.H. Kaynar, T. Aydemir, S.Ç. Kaynar, M. Ayvacıklı, An efficient removal of RB5 from aqueous solution by adsorption onto nano-ZnO/chitosan composite beads, Int. J. Biol. Macromol., 96 (2017) 459–465.
[13] Y. Liu, S. Huang, X. Zhao, Y. Zhang, Fabrication of three-dimensional porous β-cyclodextrin/chitosan functionalized graphene oxide hydrogel for methylene blue removal from aqueous solution, Colloids Surf. A, 539 (2018) 1–10.
[14] H. Mahmood, M. Tripathi, N. Pugno, A. Pegoretti, Enhancement of interfacial adhesion in glass fiber/epoxy composites by electrophoretic deposition of graphene oxide on glass fibers, Compos. Sci. Technol., 126 (2016) 149–157.
[15] G. Ersan, O.G. Apul, F. Perreault, T. Karanfil, Adsorption of organic contaminants by graphene nanosheets: a review, Water Res., 126 (2017) 385–398.
[16] O.G. Apul, Q. Wang, Y. Zhou, T. Karanfil, Adsorption of aromatic organic contaminants by graphene nanosheets: comparison with carbon nanotubes and activated carbon, Water Res., 47 (2013) 1648–1654.
[17] R. Rostamian, H. Behnejad, A comparative adsorption study of sulfamethoxazole onto graphene and graphene oxide nanosheets through equilibrium, kinetic and thermodynamic modeling, Process Saf. Environ., 102 (2016) 20–29.
[18] L. Fan, C. Luo, M. Sun, X. Li, F. Lu, H. Qiu, Preparation of novel magnetic chitosan/graphene oxide composite as effective adsorbents toward methylene blue, Bioresour. Technol., 114 (2012) 703–706.
[19] D.K. Kim, M. Hwang, D. Ko, J. Kang, K. Seong, Y. Piao, Electrochemical performance of 3D porous Ni-Co oxide with electrochemically exfoliated graphene for asymmetric supercapacitor applications, Electrochim. Acta, 246 (2017) 680–688.
[20] X. Song, Q. Shi, H. Wang, S. Liu, C. Tai, Z. Bian, Preparation of Pd-Fe/graphene catalysts by photocatalytic reduction with enhanced electrochemical oxidation-reduction properties for chlorophenols, Appl. Catal., B, 203 (2017) 442–451.
[21] S. Liu, H. Ge, C. Wang, Y. Zou, J. Liu, Agricultural waste/graphene oxide 3D bio-adsorbent for highly efficient removal of methylene blue from water pollution, Sci. Total Environ., 628–629 (2018) 959–968.
[22] T. Lu, Y. Zhu, Y. Qi, W. Wang, A. Wang, Magnetic chitosan–based adsorbent prepared *via* Pickering high internal phase emulsion for high-efficient removal of antibiotics, Int. J. Biol. Macromol., 106 (2018) 870–877.
[23] L. Maddalena, F. Carosio, J. Gomez, G. Saracco, A. Fina, Layer-by-layer assembly of efficient flame retardant coatings based on high aspect ratio graphene oxide and chitosan capable of preventing ignition of PU foam, Polym. Degrad. Stab., 152 (2018) 1–9.
[24] S. Dhanavel, N. Manivannan, N. Mathivanan, V.K. Gupta, V. Narayanan, A. Stephen, Preparation and characterization of cross-linked chitosan/palladium nanocomposites for catalytic and antibacterial activity, J. Mol. Liq., 257 (2018) 32–41.
[25] E. Bagheripour, A.R. Moghadassi, S.M. Hosseini, B.V. der Bruggen, F. Parvizian, Novel composite graphene oxide/chitosan nanoplates incorporated into PES based nanofiltration membrane: chromium removal and antifouling enhancement, J. Ind. Eng. Chem., 62 (2018) 311–320.
[26] A. Nasrullah, A.H. Bhat, A. Naeem, M.H. Isa, M. Danish, High surface area mesoporous activated carbon-alginate beads for efficient of methylene blue, Int. J. Biol. Macromol., 107 (2018) 1792–1799.
[27] T. Anitha, P. Senthil Kumar, K. Sathish Kumar, Synthesis of nano-sized chitosan blended polyvinyl alcohol for the removal of Eosin Yellow dye from aqueous solution, J. Water Process Eng., 13 (2016) 127–136.
[28] Y. Liu, L. Pan, T. Chen, X. Xu, T. Lu, Z. Sun, D.H.C. Chua, Porous carbon spheres via microwave-assisted synthesis for capacitive deionization, Electrochim. Acta, 151 (2015) 489–496.
[29] S. Suganya, P. Senthil Kumar, A. Saravanan, P. Sundar Rajan, C. Ravikumar, Computation of adsorption parameters for the removal of dye from wastewater by microwave assisted sawdust: theoretical and experimental analysis, Environ. Toxicol. Phar., 50 (2017) 45–57.
[30] P. Senthil Kumar, S. Ramalingam, C. Senthamarai, M. Niranjanaa, P. Vijayalakshmi, S. Sivanesan, Adsorption of dye from aqueous solution by cashew nut shell: studies on equilibrium isotherm, kinetics and thermodynamics of interactions, Desalination, 261 (2010) 52–60.
[31] P. Senthil Kumar, S.J. Varjani, S. Suganya, Treatment of dye wastewater using an ultrasonic aided nanoparticle stacked activated carbon: kinetic and isotherm modelling, Bioresour. Technol., 250 (2018) 716–722.
[32] C. Zhang, Z. Chen, W. Guo, C. Zhu, Y. Zou, Simple fabrication of chitosan/graphene nanoplates composite spheres for efficient adsorption of acid dyes from aqueous solution, Int. J. Biol. Macromol., 112 (2018) 1048–1054.
[33] L. Mouni, L. Belkhiri, J.C. Bollinger, A. Bouzaza, A. Assadi, A. Tirri, F. Dahmoune, K. Madani, H. Remini, Removal of Methylene Blue from aqueous solutions by adsorption on Kaolin: kinetic and equilibrium studies, Appl. Clay Sci., 153 (2018) 38–45.
[34] B. Ren, Y. Xu, L. Zhang, Z. Liu, Carbon-doped graphitic carbon nitride as environment-benign adsorbent for methylene blue adsorption: kinetics, isotherm and thermodynamics study, J. Taiwan Inst. Chem. Eng., 88 (2018) 114–120.
[35] J. Shu, R. Liu, H. Wu, Z. Liu, X. Sun, C. Tao, Adsorption of methylene blue on modified electrolytic manganese residue: kinetics, isotherm, thermodynamics and mechanism analysis, J. Taiwan Inst. Chem. Eng., 82 (2018) 351–359.
[36] G. Liu, Z. Zhang, C. Yan, Y. Wang, X. Ma, P. Gao, Y. Feng, Adsorption of estrone with few-layered boron nitride nanosheets: kinetics, thermodynamics and mechanism, Chemosphere, 207 (2018) 534–542.